View metadata, citation and similar papers at core.ac.uk
brought to you by CORE
provided by MURAL - Maynooth University Research Archive Library

Prediction of the In-Flight Radiation Patterns of the Planck Telescope

A. Martín Polegre[1], P. H. Nielsen[2], J. Tauber[3], D. Doyle[3], D. Dubruel[4], P. Martin[4], R. Daddato[3], A. Cozzani[3], V. Kirschner[3], T. Peacocke[5], H. U. Nørgaard-Nielsen[6], B. Maffei[7], A. Murphy[5], M. Sandri[8], F. Villa[8], G. Crone[3]

[1]*European Space Agency, ESTEC, Keplerlaan 1, Postbus299, 2201 AZ Noordwijk, The Netherlands,* Arturo.Martin.Polegre@esa.int

[2]*TICRA, Copenhagen K, Denmark*

[3]*European Space Agency, ESTEC, Noordwijk, The Netherlands*

[4]*Thales Alenia Space – France, Cannes-La-Bocca, France*

[5] *NUI Maynooth, Dept. of Experimental Physics, Co. Kildare, Ireland*

[6]*Danish National Space Center, Copenhagen, Denmark*

[7]*Jodrell Bank Centre for Astrophysics, The University of Manchester, United Kingdom*

[8]*INAF-IASF, Bologna, Italy*

***Abstract*— This paper summarises the work done over the last few years on the prediction of the RF performance of the Planck telescope, which was done initially to support the design phase, and later to assess compliance to specifications and to infer the in-flight performance of the telescope once in its operational orbit.**

I. Introduction

The Planck payload is a space-borne radiometer that aims at imaging the whole sky simultaneously with two scientific instruments, in nine frequency channels, between 30 GHz and 900 GHz ([1]-[4], [7], [9], [11], [12]). Its purpose is to derive a temperature anisotropy map of the cosmic background radiation remnant from the Big Bang with unprecedented sensitivity.

The ambitious goals of the Planck mission can only be met if its measurements can be calibrated to very high accuracy. The accuracy of the calibration at small angular scales depends directly on the knowledge of the radiation patterns for each detector in the focal plane of the telescope ([5], [6], [10]).

Unfortunately, the in-flight radiation patterns cannot be determined solely by measurements on ground, as the Planck operating conditions cannot be reproduced in an anechoic chamber (cryogenic temperatures, vacuum, etc.).

Therefore, the derivation of the in-flight performance must rely on an adequate combination of on-ground measurements, simulation campaigns, and, eventually, on flight data fitting.

Over more than a decade, extensive work on the prediction of the Planck radiation patterns has been done in support to the design.

This prediction work started in the very early design phase, to derive the best possible telescope configuration –eventually aplanatic, that is, two elliptical mirrors- in order to equalise as much as possible the Wave Front Error (WFE) for a large number of focal plane detector positions. In addition, simulations were also done to design an adequately shaped baffle around the telescope that attenuates unwanted sources of radiation ("straylight") that would otherwise undermine the sensitivity of the instrument.

The assessment of the performance of the flight telescope was a multidisciplinary task, as it drew expertise from the mechanical, thermal, optical and RF engineering fields.

II. Inputs to the RF Predictions

Although the optimisation of the detector positions and the telescope configuration –initially Gregorian- was done with the ray-tracing optical software CodeV, which is fast and accurate enough for that purpose, the numerical simulations of the far-field radiation pattern were carried out using the electromagnetics-modelling software package GRASP. The GRASP model was built incorporating the following geometrical and RF inputs: (a) a geometrical description of the surface details of the primary (PR) and secondary (SR) mirrors of the telescope, and of the elements surrounding the telescope (baffle, V-grooves, etc.); (b) the measured radiation patterns of the corrugated feed horns on the focal plane; and (c) alignment information to position primary and secondary mirrors relatively to each other and with respect to the focal plane assembly. For the derivation of the in-flight performance, all these inputs had to be provided at operational conditions (about 40K for the mirrors).

A. Surface shape of the mirrors

By far, the most complicated inputs to produce were the surface shapes of the mirrors. An extensive campaign of photogrammetry and interferometry measurements was conducted to characterize their surface, followed by a not less complicated post-processing work to put the measurements together.

Interferometry measurements produced the low-spatial-scale surface details, while photogrammetry provided the medium- and large-spatial-scale deformations, specially the radius of curvature, R, and conic constant, K, of the parent ellipses of the mirrors. The lack of preservation of the overall

Authorized licensed use limited to: Maynooth University Library. Downloaded on December 16,2020 at 16:33:12 UTC from IEEE Xplore. Restrictions apply.

shape of the mirrors obtained by interferometry was recovered by the determination of the mirror shape figure derived from the photogrammetry measurements.

The photogrammetry measurements were carried out from ambient temperature down to ~95K (Fig. 1). The measured trends of R and K with temperature were used to extrapolate these parameters to the operational temperature.

The interferometric measurements were conducted in a range of temperatures from ambient to ~40K for the SR (Fig. 2). However, for the PR, its large size and long focal length required the acquisition of interferograms in double-pass configuration, which increased with respect to the SR the noise caused by diffraction of light from the mirror core walls, which rendered the phase information contained in the interferograms practically useless. Only very limited areas of the PR were finally measured with this technique.

Fig. 1 The Planck telescope, prior to integration and without the horns of the focal plane. The white dots are the photogrammetry targets, which were removed before integration of the telescope into the satellite. Figure courtesy of ESA and Thales Alenia Space France.

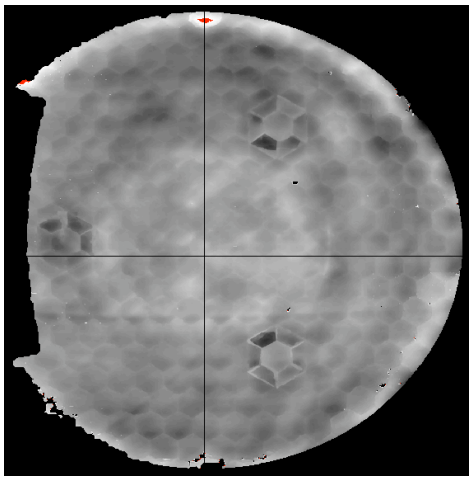

Fig. 2 Deformations at small spatial scales of the SR flight model at about 50 K as measured with 10-μm laser interferometry (the indentation at left is caused by vignetting in the interferometer optics). The grey scale is ±40 μm. The print-through of the core walls is clearly seen for most cores. The amplitude of the mirror skin inside each cell is unpredictable, as it depends on minute stress differences -caused by irregular amounts of glue between the core cell walls and the skin- that build up during cool down.

B. Radiation patterns of the focal plane feed horns

The radiation pattern of each of the single-moded feed horns (those operating below the 545-GHz band) on the focal plane was predicted using the mode-matching code CHAMP.

These patterns were calculated by the instrument teams from the measured geometrical details of the manufactured flight horns at ambient temperature, and then extrapolated at operational temperature (assuming homogeneous contraction of the material). The derived patterns were then represented in their spherical wave expansion as inputs to the GRASP model. The horns models were positioned in the expected phase centre at operational temperature. However, the simulations of the multi-moded horns (those operating at in the 545- and 857-GHz bands) were much harder to carry out and were left out of this work.

The horn patterns were all linearly polarised, so the two orthogonally polarised radiation patterns of horns corresponding to un-polarised detectors were added up in power ([8], [14]).

Mutual coupling between horns in the focal plane was considered negligible after some simulation work, which is not surprising taking into account that the horn apertures are several wavelengths in diameter and corrugated.

C. Alignment information

Simulations proved that one of the most significant factors determining the main beam shape of the telescope is the relative position and orientation of the mirrors to one another, as well as with respect to the focal plane assembly.

Therefore, theodolite measurements of targets placed on all the critical elements (reflectors, structure, focal plane) were used to tie together the coordinate frames of photogrammetry at reflector and telescope level to each other and to the spacecraft frame.

For the prediction of the in-flight performance, the best knowledge of the in-flight final alignment was used; however, it must be noted that the telescope was actually launched anti-aligned, so that, once in orbit, it would shrink to become a focused system.

D. Geometrical model of other elements

The far-out sidelobes of the radiation pattern of the telescope is determined not only by the mirrors and the horns, but also by any other element encountered by the incoming radiation before it reaches the focal plane detectors. The most important of these is the straylight baffle that surrounds the telescope. Its mission is to shield the detectors from unwanted radiation coming from directions away from those of the main beam (i.e., Solar System sources, galactic noise, etc.). Therefore, its shape determines to a high extent the level of rejection of the far-out sidelobes of the telescope´s radiation pattern.

Two models of the baffle were implemented in GRASP: one model was made of simple parts –flat surfaces connected by cylindrical sections-, and another one was built entirely as a numerical 3-D surface. While the former was used for regular simulations –it allows to reduce the simulation time

Authorized licensed use limited to: Maynooth University Library. Downloaded on December 16,2020 at 16:33:12 UTC from IEEE Xplore. Restrictions apply.

because it is relatively easy to predict the expected reflection paths of the incoming rays-, the latter was used to make sure that no radiation leaked between the parts of the piece-wise model –avoiding fake peaks in the simulated radiation pattern.

Other parts, such as the V-grooves, the solar array, and the lateral spacecraft service module faces, were also built into the GRASP model. Fig. 3 shows some of the elements of the spacecraft built into GRASP.

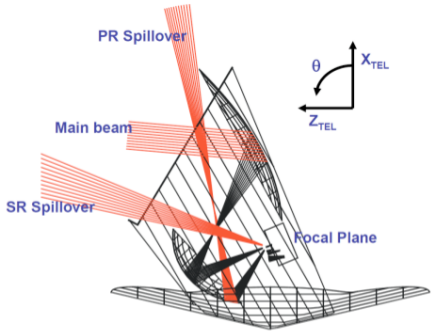

Fig. 3 Sketch of the GRASP model of the telescope, baffle and first V-groove, showing the direction of the main beam and spillover lobes of the radiation patterns.

III. Simulation Methods

The prediction of the radiation pattern of the telescope per detector was done using both Physical Optics (PO) and the Multi-Ray Geometrical Theory of Diffraction (MR-GTD) techniques available in GRASP.

The main beams were derived using only PO, as GTD would fail in that angular region. However, being PO a very time-consuming method, GTD was used for the prediction of the sidelobes of the patterns.

In order to build confidence in the process of estimating the flight predictions, a full-scale qualification model of the Planck telescope and surrounding baffle ("RFQM") was built and subjected to a measurement campaign.

The objectives of this campaign were to: (a) measure the qualitative RF properties of the system; and (b) validate the ability to use GRASP to make a prediction of the flight patterns based on geometrical information.

Many of the discrepancies found between the predicted and measured RFQM patterns (see Fig. 4) were corrected by means of (a) adding geometrical objects to the GRASP model which had been neglected *a priori* (for example, the improvement of the V-groove floor reflections, and the addition of side panels of the focal plane assembly as scatterers); (b) replacing parts of the pattern suffering from GTD-induced caustics by PO calculations; (c) adding more reflected and diffracted rays to the family of rays propagated by GRASP when using the GTD technique; and (d) identifying and ignoring "fictitious" pattern peaks produced by reflections on the anechoic chamber walls.

The main results of this campaign were: (a) a GRASP model that can be applied to the geometry of the flight reflectors (referred to as FM for "Flight Model"); and (b) the difference between predicted and measured patterns, which provides a quantitative measure of the uncertainty in the modelling based on ground information.

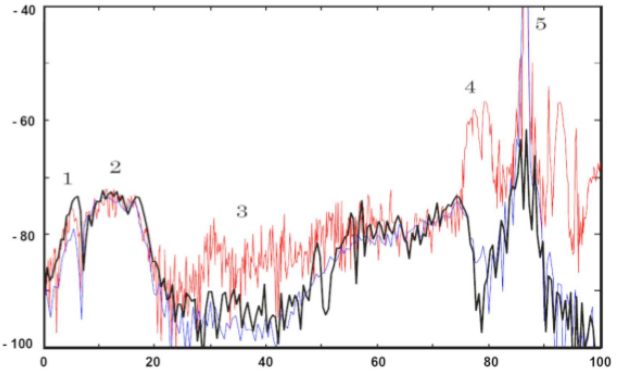

Fig. 4 Cut in the radiation pattern at 100 GHz in the elevation direction through the beam peak; the horizontal axis is in degrees, the peak of the main beam is at 85°. The vertical axis is in dB from peak (which is 61.5 dBi at 100 GHz). The measured level is shown in red, the initial model in blue and the improved model in black. The regions labelled 1 and 2 show the SR spillover (see Fig. 3). Region 1 shows an area where PO corrections are required to the GTD model. The area labelled 3 shows a region where there is poor correlation between the model and the measurement; this lack of correlation could be due to the presence of dust on the reflectors. Regions 4 and 5 correspond to artificial peaks produced by known artifacts created by features of the CATR reflectors (edge serrations, etc.). Note that the main lobe is not well represented by this (multi-GTD) model which is specifically built for the calculation of the full-sphere radiation pattern.

IV. Results

Hundreds of radiation patterns were calculated, including all main beams (polarised and un-polarised) at various frequencies in each band, and many full-sphere patterns, some of them at several frequencies in band. Some examples are depicted in Fig. 5 and Fig. 6.

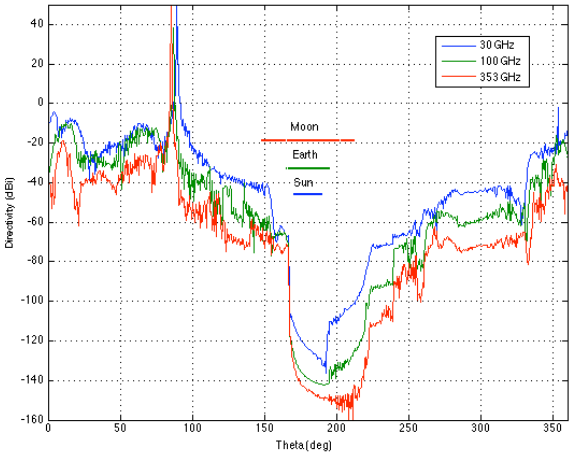

Fig. 5 Three cuts through the main beam in the telescope symmetry plane (φ = 0◦ in Fig. 5) at 30, 100 and 353 GHz. The horizontal axis is θ as in Fig. 3; the vertical axis is in dBi. The horizontal lines show the levels at which Sun, Moon and Earth would induce a signal of 1 μK in the detectors; and the angular regions where each object has an influence.

Authorized licensed use limited to: Maynooth University Library. Downloaded on December 16,2020 at 16:33:12 UTC from IEEE Xplore. Restrictions apply.

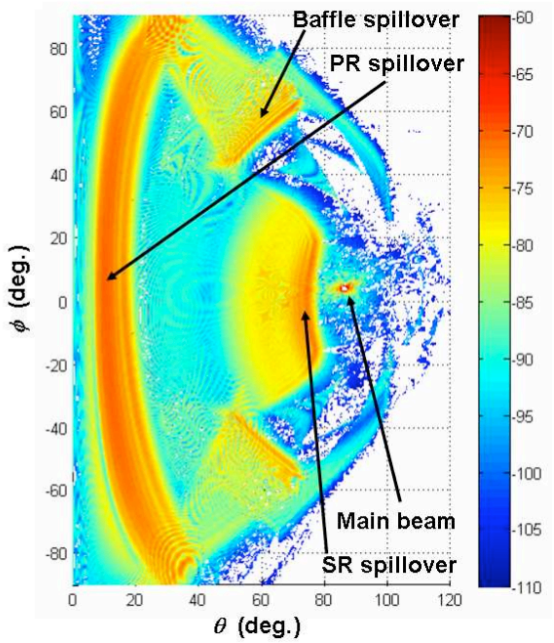

Fig. 6 A typical far side lobe pattern for Planck (in this case at 100 GHz), showing the main features of interest. The horizontal axis corresponds to the angle around −YT E L in Fig. 3, and the vertical axis is the angle around −XT E L ; the spin axis is at (0, 0). The color scale is in dB from peak (note that the color scale is cut off at -60 dB from peak). The main beam is located at ~85º from the spin axis. The "SR spillover" is power from the sky that reaches the feed horn without going through the telescope, mostly concentrated in the region over the top of the SR. The "PR spillover" is power from the sky that bypasses the PR, and then reflects on the SR to reach the feed horn; it is concentrated in the region over the top of the PR. The "Baffle spillover" is power from the sky which reflects on the inside of the baffle and then reaches the feed horn via reflection on the SR.

V. Uncertainties Associated to the Predictions

The level of accuracy of the obtained results depends not only on the level of accuracy of the prediction software and on that of the built RF model, but also on the level of uncertainty associated to the inputs.

The alignment of the mirrors is the dominant component of the flight prediction uncertainty. The alignment depends on a dozen partly-dependent parameters (translations, rotations and deformations of the reflectors, telescope structure, and focal plane). For the same optical performance of the telescope, expressed in terms of WFE, the RF pattern calculated can vary widely for different combinations of parameters. Therefore the selection of what values to select for the parameters of best- and worst-case alignments is not trivial. A Monte-Carlo simulation was used to determine the occurrence likelihood of all cases in the WFE-defocus plane. Within the 68% likelihood contour, the selected best case was that which minimized the WFE with the largest defocus, and had the smallest parameter variations from the as-built case (and therefore the largest probability of occurrence). Similarly, the worst case was selected to be that which maximized WFE with the largest defocus. Since defocus has the lowest-order angular aberration effect on the main beam, this selection provides an "envelope" for higher mode parameter combinations.

Fig. 7 shows the difference between best- and worst-case patterns for one of the horns at 353 GHz. The maximum differences are observed in the SR spillover region.

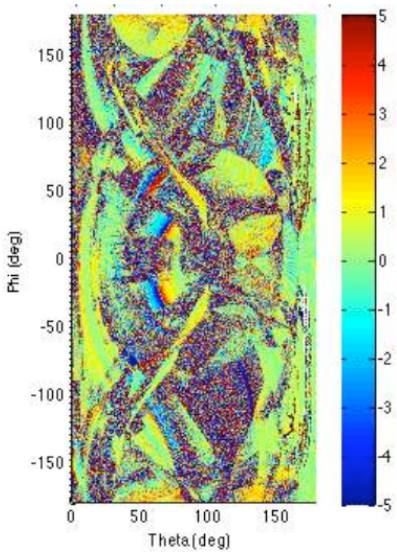

Fig. 7 Difference between best- and worst-case patterns for horn number 6 at 353 GHz. The color scale shows differences between -5 and +5 dB. The largest uncertainties are associated to the SR spillover lobes.

VI. In-Flight Characterisation

The improvement of the flight predictions can at this stage only be achieved through the utilisation of the in-flight acquired data. It is expected that isolating in-flight acquired data when the main beams scan through a bright point source - such as Mars or Jupiter- will be useful to derive the in-flight alignment parameters of the telescope, taking into account that the same source will be seen by all detectors (although not simultaneously) and at various frequencies. The optimisation of the alignment of the telescope to match the obtained in-flight main beam patterns will allow for a better knowledge of the alignment parameters and therefore for a reduction of the uncertainty of the pattern shape at lower levels.

VII. Other Factors

The potential effect of other factors on the flight radiation pattern have also been studied:

(a) the wide-band response of the detectors (around 30%), which tends to fill up the nulls and to smooth the radiation patterns; the wide-band nature of the detectors was accounted for by power-averaging the patterns calculated at several (between 5 and 7) frequencies;

(b) the effect of dust particles deposited on the mirrors in the period between the last cleaning operation and the launch: this effect is more important at the higher frequency bands, but the uncertainty associated to the particle distribution and to the analysis method is large;

Authorized licensed use limited to: Maynooth University Library. Downloaded on December 16,2020 at 16:33:12 UTC from IEEE Xplore. Restrictions apply.

(c) the effect of the spacecraft self-emission on the received signals. The payload and satellite radiate thermally within the detector bandwidths; if the radiating surface is fluctuating in temperature or emissivity, then it will translate into a corresponding signal fluctuation at the detector. This is referred to as self-emission. The amplitude of the detected signal depends on the amplitude of the temperature fluctuation, the emissivity of the surface, and on the RF coupling of the surface to the detector. The most troublesome self-emission signals are those which are synchronised to the satellite spin rate or one of its harmonics. According to the analysis done, self-emission levels are very low and do not affect meaningfully the instrument sensitivity.

(d) the effect of the mirror core walls in the radiation pattern is not as worrisome as initially thought, due to the irregular amplitude of the cells, which smears the power contained in the grating lobes of this periodic structure.

VIII. Conclusions

The conclusions that can be drawn from this work are:

(a) the major characteristics of the main beams are within requirements;

(c) the reliability of the GRASP models of the beam shapes has been verified to high accuracy;

(d) the range of potential misalignments is such that the in-flight measurements can be used to correlate the GRASP main beam models to high accuracy. The optimised model can be used to extend the beam shape knowledge to levels far below those directly measurable in flight.

The ground activities have provided an adequate starting point for the in-flight optical calibration activities, which complement them. The current expectation is that with the combination of ground knowledge and flight measurements, Planck will be able to achieve its main requirements in terms of RF knowledge.

Acknowledgment

The authors acknowledge the involvement and dedication to this work of many people: from colleagues with Thales Alenia Space - France, responsible for the telescope and for the Planck spacecraft; from the instrument teams, which provided the LFI and HFI instruments; from the Danish Space Research Centre, which provided the mirrors manufactured by ASTRIUM GmbH; to many colleagues who spent sleepless nights during holiday periods in an anechoic chamber. This list is only a small sample.

References

[1] A. J. Tauber *et al*, "Planck pre-launch status: the Planck mission", submitted to *Astronomy and Astrophysics*, 2009.

[2] A. J. Tauber *et al*, "Planck pre-launch status: the optical system", submitted to *Astronomy and Astrophysics*, 2009.

[3] N. Mandolesi *et al*., "Planck pre-launch status: the Planck-LFI programme", submitted to *Astronomy and Astrophysics*, 2009.

[4] M. Bersanelli *et al*., "Planck pre-launch status: design and description of the low-frequency instrument", submitted to *Astronomy and Astrophysics*, 2009.

[5] A. Mennella *et al*., "Planck pre-launch status: low frequency instrument calibration and scientific performance", submitted to *Astronomy and Astrophysics*, 2009.

[6] F. Villa *et al*., "Planck pre-launch status: calibration of LFI flight model radiometers", submitted to *Astronomy and Astrophysics*, 2009.

[7] M. Sandri *et al*., "Planck pre-launch status: LFI Optics", submitted to *Astronomy and Astrophysics*, 2009.

[8] P. Leahy *et al*., "Planck pre-launch status: expected LFI polarization capability", submitted to *Astronomy and Astrophysics*, 2009.

[9] J.-M. Lamarre *et al*., "Planck pre-launch status: the HFI instrument, from specification to actual performance", submitted to *Astronomy and Astrophysics*, 2009.

[10] F. Pajot *et al*., "Planck pre-launch status: HFI ground calibration", submitted to *Astronomy and Astrophysics*, 2009.

[11] P. A. R. Ade *et al*., "Planck pre-launch status: the optical architecture of the HFI", submitted to *Astronomy and Astrophysics*, 2009.

[12] W. Holmes *et al*., "Planck pre-launch status: initial test results on Bolometers for the Planck High Frequency Instrument", submitted to *Astronomy and Astrophysics*, 2009.

[13] B. Maffei *et al*., "Planck pre-launch status: HFI beam expectations patterns from the optical optimization of the focal plane", submitted to *Astronomy and Astrophysics*, 2009.

[14] C. Rosset *et al*., "Planck pre-launch status: HFI polarization characteristics", submitted to *Astronomy and Astrophysics*, 2009.

Authorized licensed use limited to: Maynooth University Library. Downloaded on December 16,2020 at 16:33:12 UTC from IEEE Xplore. Restrictions apply.